

# Magnetic and tunneling magnetoresistive properties of an all-oxide $\text{Fe}_3\text{O}_4\text{-Al}_2\text{O}_3$ granular system

D. Tripathy and A. O. Adeyeye\*

*Information Storage Materials Laboratory, Department of Electrical and Computer Engineering,  
National University of Singapore, Singapore 117576*

S. Shannigrahi

*Institute of Materials Research and Engineering, 3 Research Link, Singapore 117602*

(Received 3 June 2007; revised manuscript received 23 August 2007; published 16 November 2007)

A systematic study on the structural, magnetic, and transport properties of an all-oxide granular system consisting of  $\text{Fe}_3\text{O}_4$  grains dispersed in an insulating  $\text{Al}_2\text{O}_3$  matrix is presented. X-ray diffraction and transmission electron microscopy analyses provide the structure of nanosized  $\text{Fe}_3\text{O}_4$  grains embedded in an amorphous  $\text{Al}_2\text{O}_3$  matrix and confirm that the  $\text{Fe}_3\text{O}_4$  grain size decreases with increasing  $\text{Al}_2\text{O}_3$  volume fraction  $x$ . Magnetic measurements further show that the coercivity of the granular films decreases with increasing  $x$  due to decreasing  $\text{Fe}_3\text{O}_4$  grain size, with the magnetization curves exhibiting typical superparamagnetic characteristics for  $x > 0.19$ . Temperature dependence of resistance and nonlinearity in current-voltage characteristics confirms that the spin dependent tunneling of conduction electrons across grains dominates the transport properties. This tunneling conductance depends on the relative orientation of magnetization between  $\text{Fe}_3\text{O}_4$  grains, which results in an isotropic granular tunneling magnetoresistance (TMR) effect. We also observed that the granular TMR ratio has strong temperature dependence and decreases with increasing temperature for all the granular films.

DOI: [10.1103/PhysRevB.76.174429](https://doi.org/10.1103/PhysRevB.76.174429)

PACS number(s): 75.47.De, 72.25.-b, 73.40.Gk, 74.25.Ha

## I. INTRODUCTION

The giant magnetoresistance (GMR) effect has been extensively investigated since it was discovered in Fe/Cr multilayers<sup>1</sup> and subsequently in magnetic heterogeneous alloys with ferromagnetic grains dispersed in a nonmagnetic metallic matrix.<sup>2</sup> The mechanism of GMR is believed to be a manifestation of the conduction electrons' spin dependent scattering dependence on the local magnetic configuration.<sup>3</sup> A similar magnetoresistance (MR) effect that was observed in granular metals embedded in an insulating medium has been interpreted to be a consequence of spin dependent tunneling between adjacent grains<sup>4</sup> and is termed as a granular tunneling magnetoresistance (TMR) effect. These new perspectives have led to the investigation of various insulating granular systems with remarkable TMR values.

Heterogeneous Fe-SiO<sub>2</sub> granular films, for example, exhibit superparamagnetic nature, and a TMR ratio of 1.5% at room temperature has been reported for Fe volume fractions smaller than 45%.<sup>5</sup> The volume fraction dependence of the TMR ratio for these films was explained on the basis of the distance between the nearest neighbor granular surfaces. An enhanced TMR ratio of 20.1% was observed in Fe-Al<sub>2</sub>O<sub>3</sub> granular films at 5 K and was attributed to spin dependent cotunneling in the Coulomb blockade regime along with suppression of spin-flip processes with decreasing temperature.<sup>6</sup> TMR values up to 7.5% at 78 K have also been obtained for Fe-MgF<sub>2</sub> films, and the field dependence of the TMR has been well described by the form proportional to the square of magnetization.<sup>7</sup> The TMR effect in this system was isotropic in nature and results from the tunneling conductance depending on the relative magnetizations of neighboring particles. Strijkers *et al.*<sup>8</sup> have investigated the temperature dependent TMR in FeHfO and FeHfSiO granular films and observed an unusual dependence which could not be explained only by

spin dependent tunneling. The temperature dependence was described by a two current model which takes into account spin-flip scattering in the amorphous FeHf(Si)O matrix. A large TMR of magnitude 158% was also observed at room temperature in a polycrystalline Zn<sub>0.41</sub>Fe<sub>2.59</sub>O<sub>4</sub> sample, in which the Zn<sub>0.41</sub>Fe<sub>2.59</sub>O<sub>4</sub> grains are separated by insulating  $\alpha\text{-Fe}_2\text{O}_3$  boundaries.<sup>9</sup> The huge room-temperature TMR is attributed to the high spin polarization of Zn<sub>0.41</sub>Fe<sub>2.59</sub>O<sub>4</sub> grains and antiferromagnetic (AF) correlations between magnetic domains on both sides of the insulating  $\alpha\text{-Fe}_2\text{O}_3$  boundary.

On the other hand, while ferromagnetic oxides such as  $\text{Fe}_3\text{O}_4$  have been predicted to be half metallic by band structure calculations,<sup>10</sup> the room-temperature TMR for tunnel junctions with  $\text{Fe}_3\text{O}_4$  electrodes and tunnel barriers such as MgO,<sup>11</sup> CoCr<sub>2</sub>O<sub>4</sub>,<sup>12</sup> or SrTiO<sub>3</sub> (Ref. 13) has been negligible, especially when compared with room-temperature TMR ratios of more than 200% in tunnel junctions comprising of 3d metals and MgO crystalline barriers.<sup>14</sup> However, tunnel junctions incorporating  $\text{Fe}_3\text{O}_4$  as one of the electrodes and  $\text{Al}_2\text{O}_3$  as the tunnel barrier have shown some improvement and exhibit positive TMR ratios of more than 10% at room temperature.<sup>15-18</sup> This led to elaborate studies on the physical properties of fully epitaxial  $\text{Fe}_3\text{O}_4/\text{Al}_2\text{O}_3$  bilayers to be included in magnetic tunnel junctions.<sup>19</sup> Recently, experiments focused to obtain direct insight into the spin polarization at the  $\text{Fe}_3\text{O}_4/\text{Al}_2\text{O}_3$  interface by using spin-resolved photoelectron spectroscopy have yielded a negative spin polarization of -40%.<sup>20</sup> Moreover,  $\text{Fe}_3\text{O}_4\text{-SiO}_2$  composite films which form a granular structure also exhibit spin dependent tunneling transport properties.<sup>21</sup> Recently, it was observed that polystyrene coated  $\text{Fe}_3\text{O}_4$  nanoparticles exhibit a TMR ratio of 22.8% at room temperature as a consequence of intergranular tunneling.<sup>22</sup>

The  $\text{Fe}_3\text{O}_4/\text{Al}_2\text{O}_3$  system thus presents an extremely interesting study for investigating physical mechanisms. To the best of our knowledge, the physical properties of a granular system incorporating highly spin polarized  $\text{Fe}_3\text{O}_4$  embedded in an insulating  $\text{Al}_2\text{O}_3$  matrix have not yet been reported. A detailed study of the structural and temperature dependent tunneling magnetotransport properties of  $\text{Fe}_3\text{O}_4\text{-Al}_2\text{O}_3$  granular films is thus essential. In this work, we present a systematic and comprehensive study of the microstructural, magnetic, and transport properties of a  $\text{Fe}_3\text{O}_4\text{-Al}_2\text{O}_3$  granular system prepared by cosputtering technique. We observed that the granular films are extremely sensitive to the  $\text{Al}_2\text{O}_3$  volume fraction  $x$  and exhibit marked changes as  $x$  is varied.

## II. EXPERIMENTAL DETAILS

$(\text{Fe}_3\text{O}_4)_{1-x}(\text{Al}_2\text{O}_3)_x$  granular films were deposited on pre-cleaned Si(100) substrates by reactively sputtering Fe (dc) and  $\text{Al}_2\text{O}_3$  (rf) targets in an Ar+ $\text{O}_2$  mixture at room temperature. The base pressure of the chamber was better than  $3 \times 10^{-8}$  Torr before deposition. The films were then annealed at 300 °C for 30 min without breaking the vacuum to remove phases of paramagnetic FeO which may have been formed during reactive sputtering of Fe.<sup>23</sup> Microstructural properties and crystalline structure of the films were examined by conventional  $\theta\text{-}2\theta$  x-ray diffraction (XRD) scans using Cu  $K\alpha$  radiation and transmission electron microscopy (TEM). Chemical states and composition were further analyzed using x-ray photoelectron spectroscopy (XPS) using an Al  $K\alpha$  source. Magnetic properties were characterized using a vibrating sample magnetometer. Electrical contacts to the films were made using standard optical lithography, metallization of 200 nm Al, followed by lift-off in acetone. The transport properties of the films were measured using the standard four-probe dc technique.

## III. RESULTS AND DISCUSSION

### A. Structural and chemical properties

Typical  $\theta\text{-}2\theta$  XRD scans for  $(\text{Fe}_3\text{O}_4)_{1-x}(\text{Al}_2\text{O}_3)_x$  films as a function of  $\text{Al}_2\text{O}_3$  volume fraction  $x$  are shown in Fig. 1. The films are polycrystalline and all peaks can be assigned to the inverse cubic spinel structure of  $\text{Fe}_3\text{O}_4$ . We also note that since no peaks corresponding to crystalline  $\text{Al}_2\text{O}_3$  were detected in the XRD scans, the  $\text{Al}_2\text{O}_3$  in our granular system is amorphous in nature. With increasing  $x$ , the peak intensities weaken and the widths become progressively broader, indicating that the addition of  $\text{Al}_2\text{O}_3$  significantly hinders the grain growth of  $\text{Fe}_3\text{O}_4$ . According to Scherrer's formula, the average grain size  $D$  is given by<sup>24</sup>

$$D = \frac{k\lambda}{\beta_{\text{eff}} \cos \theta}, \quad (1)$$

where  $k$  is the particle shape factor (generally taken as 0.9),  $\lambda$  is the wavelength of Cu  $K\alpha$  radiation,  $2\theta$  is the XRD peak position with maximum intensity, and  $\beta_{\text{eff}}$  is defined as  $\beta_{\text{eff}}^2 = \beta_m^2 - \beta_s^2$ , where  $\beta_m$  is the experimental full width at half maximum (FWHM) for the measured sample and  $\beta_s$  is the

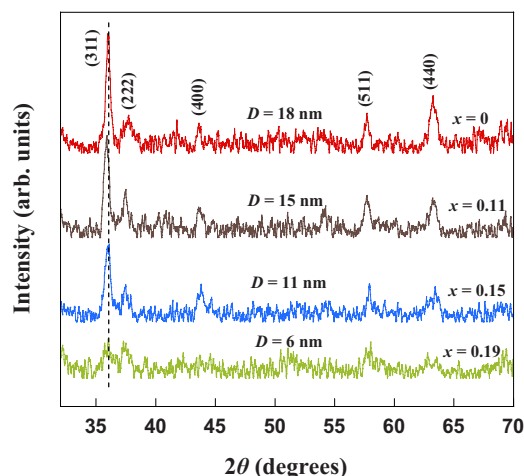


FIG. 1. (Color online) XRD patterns for  $(\text{Fe}_3\text{O}_4)_{1-x}(\text{Al}_2\text{O}_3)_x$  films as a function of  $x$ .

FWHM for a standard silicon sample. Using the peak position at  $2\theta = 35.45^\circ$  and FWHM for the (311) peak, the  $\text{Fe}_3\text{O}_4$  average grain was determined and it was observed that the grain size decreases from  $\sim 18$  nm for  $x=0$  to  $\sim 6$  nm for  $x=0.19$ . The peak intensities become too small to be detected for  $x > 0.19$ .

Figure 2 displays the bright field TEM images and the selected area diffraction (SAED) patterns for the  $(\text{Fe}_3\text{O}_4)_{1-x}(\text{Al}_2\text{O}_3)_x$  films with  $x=0, 0.11$ , and  $0.19$ , respectively. It can be clearly seen that for undoped  $\text{Fe}_3\text{O}_4$  films ( $x=0$ ), the grains are well defined and separated by a large density of grain boundaries. For  $x=0.11$  and  $x=0.19$ , the grain size reduces, as shown in Figs. 2(b) and 2(c), respectively. The high resolution TEM images reveal a well defined granular structure in which polycrystalline  $\text{Fe}_3\text{O}_4$  grains are surrounded by amorphous insulating barriers (clearly distinguishable from the bright contrast). With increasing  $x$ , the  $\text{Fe}_3\text{O}_4$  grain size is significantly reduced, and the grains distribute uniformly in the amorphous  $\text{Al}_2\text{O}_3$  matrix. We have estimated the mean grain size  $D$  and the standard deviation  $\sigma_D$  using the linear intercept technique on the bright field TEM images and tabulated the results in Table I. It can be clearly seen that the grain sizes estimated from the TEM images are in good agreement with those calculated from the XRD patterns. The rings in the SAED patterns can be indexed to polycrystalline  $\text{Fe}_3\text{O}_4$ , in accordance with the XRD results, while the bright spots represent the crystalline orientations of the Si substrate. Moreover, we also observed that the SAED pattern corresponding to  $x=0.19$  shows the existence of diffused halo rings, which are indicative of an increasingly amorphous microstructure as the  $\text{Al}_2\text{O}_3$  content in the granular films is increased.

It should be noted that  $\text{Fe}_3\text{O}_4$  has the same cubic inverse spinel structure and nearly identical lattice parameter as  $\gamma\text{-Fe}_2\text{O}_3$ . Hence, in most cases, it is extremely difficult to distinguish between the two by XRD and TEM characterizations. To further investigate the composition of the granular films, systematic XPS measurements were performed. Figure 3 shows the Al 2p and Fe 2p core level XPS spectra for the  $(\text{Fe}_3\text{O}_4)_{1-x}(\text{Al}_2\text{O}_3)_x$  films. We observed that the binding en-

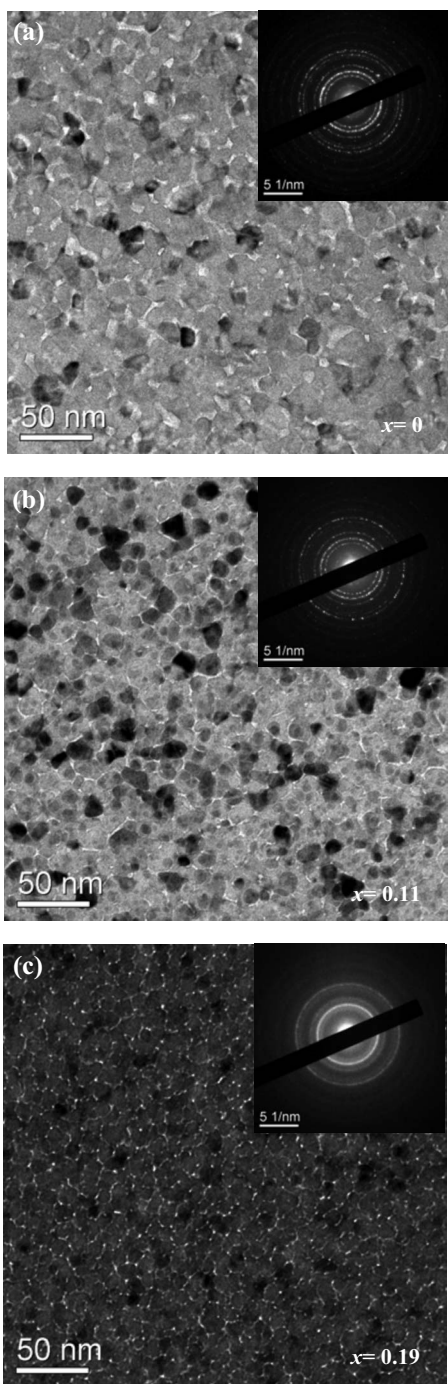


FIG. 2. TEM bright field images for  $(\text{Fe}_3\text{O}_4)_{1-x}(\text{Al}_2\text{O}_3)_x$  films as a function of  $x$ . Insets show the corresponding SAED patterns.

ergy of the Al  $2p$  core level occurs at 74 eV for all the films with  $x > 0$ . This observation is in good agreement with the binding energy of oxidized Al, as compared to a binding energy of 72 eV for metallic Al.<sup>19</sup> The Fe  $2p$  line shape is rather complex, and satellite peaks caused by the charge transfer allow for the identification of the Fe oxidation state. Due to spin orbit coupling, the Fe  $2p$  core levels split into  $2p_{1/2}$  and  $2p_{3/2}$  components. Figure 3(b) shows that for  $x = 0$ , the Fe  $2p_{3/2}$  and  $2p_{1/2}$  peaks are broadened and situated at  $\sim 711$  and  $\sim 725$  eV, respectively, with the absence of

TABLE I. Mean and standard deviation of the grain size for  $(\text{Fe}_3\text{O}_4)_{1-x}(\text{Al}_2\text{O}_3)_x$  films.

$x$	Mean grain size $D$ (nm)	Standard deviation $\sigma_D$ (nm)
0	17.2	1.8
0.11	15.5	1.3
0.19	5.3	1.4

satellite peaks occurring at 719 eV. Such satellite peaks occurring at a binding energy of 719 eV are characteristic of  $\text{Fe}^{3+}$  in  $\gamma\text{-Fe}_2\text{O}_3$ . We can thus confirm the formation of stoichiometric  $\text{Fe}_3\text{O}_4$  for  $x=0$ .<sup>21,22</sup> For  $x=0.11$ , however, we observed an extremely small satellite peak at 719 eV. This may possibly be due to small traces of  $\text{Fe}^{3+}$  rich oxide present in the  $\text{Fe}_3\text{O}_4\text{-Al}_2\text{O}_3$  films for  $x > 0$ , due to bonding between oxygen in  $\text{Al}_2\text{O}_3$  and  $\text{Fe}^{2+}$  ions in  $\text{Fe}_3\text{O}_4$ . Hence, interfacial reactions occurring in the  $\text{Fe}_3\text{O}_4\text{-Al}_2\text{O}_3$  films result in a small degree of nonstoichiometry at the interface between  $\text{Fe}_3\text{O}_4$  grains and the  $\text{Al}_2\text{O}_3$  matrix.

**B. Electrical transport and  $I$ - $V$  characteristics**

Figure 4(a) shows the temperature dependence of electrical resistivity under zero magnetic field for

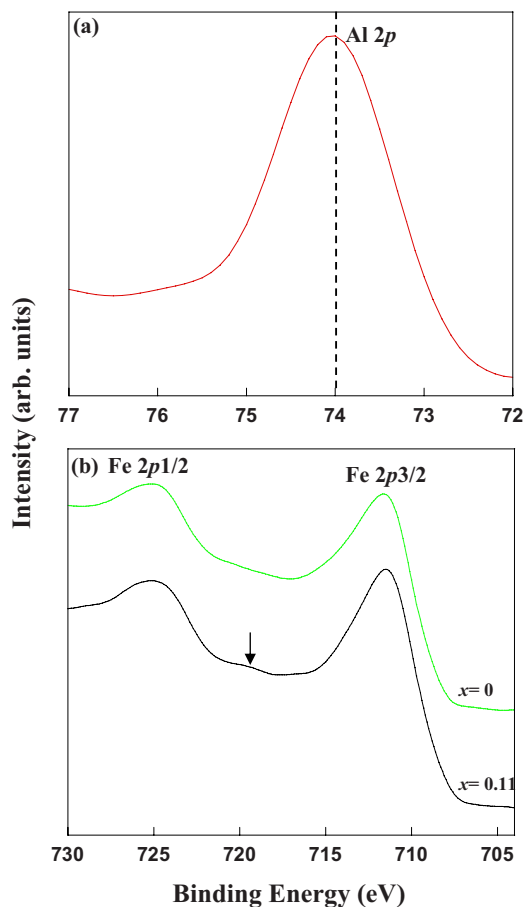


FIG. 3. (Color online) (a) Al  $2p$  core level XPS spectrum characteristic of all  $(\text{Fe}_3\text{O}_4)_{1-x}(\text{Al}_2\text{O}_3)_x$  films with  $x > 0$ , and (b) Fe  $2p$  core level XPS spectrum for  $(\text{Fe}_3\text{O}_4)_{1-x}(\text{Al}_2\text{O}_3)_x$  films.

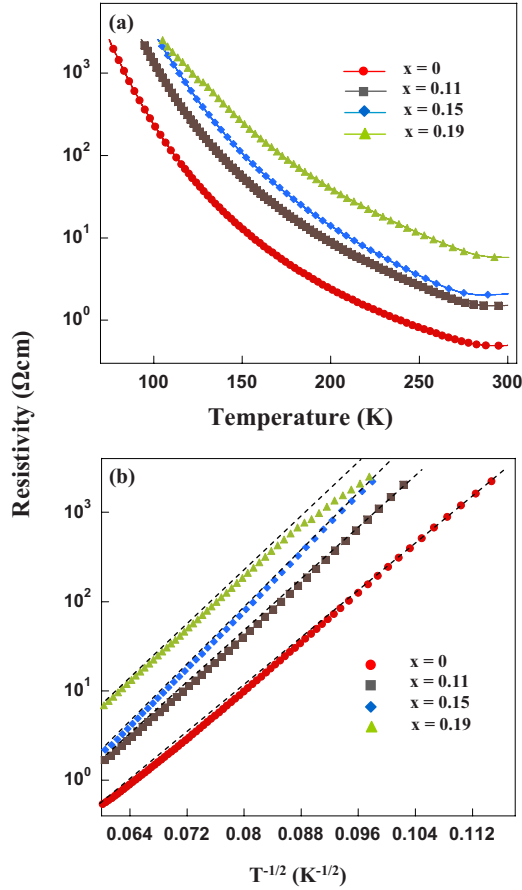


FIG. 4. (Color online) (a) Resistivity vs temperature, and (b)  $\log R$  vs  $T^{-1/2}$  for  $(\text{Fe}_3\text{O}_4)_{1-x}(\text{Al}_2\text{O}_3)_x$  films as a function of  $x$ .

$(\text{Fe}_3\text{O}_4)_{1-x}(\text{Al}_2\text{O}_3)_x$  films. We observed that with increasing Al<sub>2</sub>O<sub>3</sub> concentration, the room-temperature resistivity increases from  $0.5 \Omega\text{cm}$  ( $x=0$ ) to  $7.2 \Omega\text{cm}$  ( $x=0.19$ ). The low resistivity for films with  $x=0$  can be attributed to the conduction network of closely packed Fe<sub>3</sub>O<sub>4</sub> grains. As  $x$  is increased, the enhancement of room-temperature resistivity results from the fact that the Fe<sub>3</sub>O<sub>4</sub> grains become increasingly isolated electrically as the conduction network is broken by the insulating Al<sub>2</sub>O<sub>3</sub> component in the granular films. Another striking feature which is evident from Fig. 4(a) is that the intrinsic Verwey transition,<sup>25</sup> which is usually observed in Fe<sub>3</sub>O<sub>4</sub>, does not appear for any of the films. This suggests that the measured resistivity of our films is an extrinsic transport property and is dominated by grain boundaries or insulating tunnel barriers.<sup>21</sup> The disappearance of Verwey transition in thin films has been attributed to a variety of factors such as substrate induced stress, large density of grain boundaries, and the small size of ferromagnetic grains or domains.<sup>26,27</sup>

In Fig. 4(b), we replot the temperature dependence of resistivity as  $\log \rho$  vs  $T^{-1/2}$ . We observed that there is an extremely good linear agreement between  $\log \rho$  and  $T^{-1/2}$  for all our films. For  $x=0$ , this linear relation indicates a tunneling mechanism of electrons across grain boundaries separating adjacent Fe<sub>3</sub>O<sub>4</sub> grains.<sup>26,28–30</sup> The grain boundaries thus act as tunnel barriers for current conduction for  $x=0$ . This

relation was first obtained by Sheng *et al.*<sup>31</sup> by considering the influence of tunneling and thermal activation on the conduction mechanism in insulating granular systems. For the temperature dependence of resistivity for  $(\text{Fe}_3\text{O}_4)_{1-x}(\text{Al}_2\text{O}_3)_x$  films, similar behavior has also been observed for other insulating granular systems, and the resistivity has been expressed as<sup>4,6,21,32</sup>

$$\rho = \rho_0 \exp\{2(C/k_B)^{1/2}T^{-1/2}\}, \quad (2)$$

$$C = (2\pi/h)(2m\varphi)^{1/2}sE_c, \quad (3)$$

$$E_c = (e^2/\varepsilon\langle d \rangle)\{2/(1 + \langle d \rangle/2\langle s \rangle)\}, \quad (4)$$

where  $C$  is the activation energy,  $k_B$  is Boltzmann's constant,  $h$  is Planck's constant,  $m$  is effective electron mass,  $\varphi$  is effective barrier height,  $s$  is separation between the grains,  $E_c$  is the charging energy,  $e$  is the electron charge,  $\varepsilon$  is the dielectric constant of Al<sub>2</sub>O<sub>3</sub>,  $\langle d \rangle$  is the average grain size, and  $\langle s \rangle$  is the average grain separation. We can clearly see that the slopes of the linear plots in Fig. 4(b) are strongly dependent on the Al<sub>2</sub>O<sub>3</sub> volume fraction  $x$ . Our structural characterizations have shown that the average grain size  $\langle d \rangle$  decreases from 15.5 to 5.3 nm, while the average grain separation  $\langle s \rangle$  increases approximately from 1.5 to 1.8 nm as  $x$  is increased from 0.11 to 0.19. The charging energy  $E_c$  increases from 0.044 to 0.25 eV in accordance with Eq. (4), and hence the slope of the plots given by  $2(C/k_B)^{1/2}$  also increases. From the gradient of the plots in Fig. 4(b), we have estimated that  $C$  increases from 0.334 to 0.432 eV as  $x$  is increased from 0.11 to 0.19. Using  $\varepsilon=9\varepsilon_0$  for Al<sub>2</sub>O<sub>3</sub> in Eq. (3), we have estimated the average value of the barrier height  $\varphi$  to be  $\sim 0.96$  eV. Although this value is lower than the Al<sub>2</sub>O<sub>3</sub> gap ( $\sim 8$  eV), it is consistent with the effective barrier height obtained on “sandwich” tunnel junctions consisting of an amorphous Al<sub>2</sub>O<sub>3</sub> barrier.

To further our understanding on the conduction mechanism in the  $(\text{Fe}_3\text{O}_4)_{1-x}(\text{Al}_2\text{O}_3)_x$  films, we have systematically measured the  $I$ - $V$  curves as a function of temperature. Figure 5 clearly shows that for  $x=0$ , all the  $I$ - $V$  curves are linear, thus representing an Ohmic conduction mechanism with resistivity increasing monotonically with decreasing temperature. With increasing  $x$ , however, the  $I$ - $V$  curves deviate from their Ohmic behavior and exhibit highly nonlinear features which are characteristic of electron tunneling across insulating barriers. The nonlinearity in the curves increases with decreasing temperature for  $x=0.15$  and  $x=0.19$ , respectively. Interestingly, it was also observed that for  $x=0.19$  at 150 K, the tunneling current is almost negligible for  $V < 0.35$  V and increases gradually as  $V$  exceeds 0.35 V. More quantitatively, the low voltage resistance for  $x=0.19$  increases dramatically below 150 K. This large increase in tunnel resistance at low temperatures for  $x=0.19$  may be ascribed to the onset of the Coulomb blockade effect in the  $(\text{Fe}_3\text{O}_4)_{1-x}(\text{Al}_2\text{O}_3)_x$  films.<sup>33</sup>

### C. Magnetic properties

Figure 6(a) shows the representative room-temperature magnetization curves for the  $(\text{Fe}_3\text{O}_4)_{1-x}(\text{Al}_2\text{O}_3)_x$  films as a

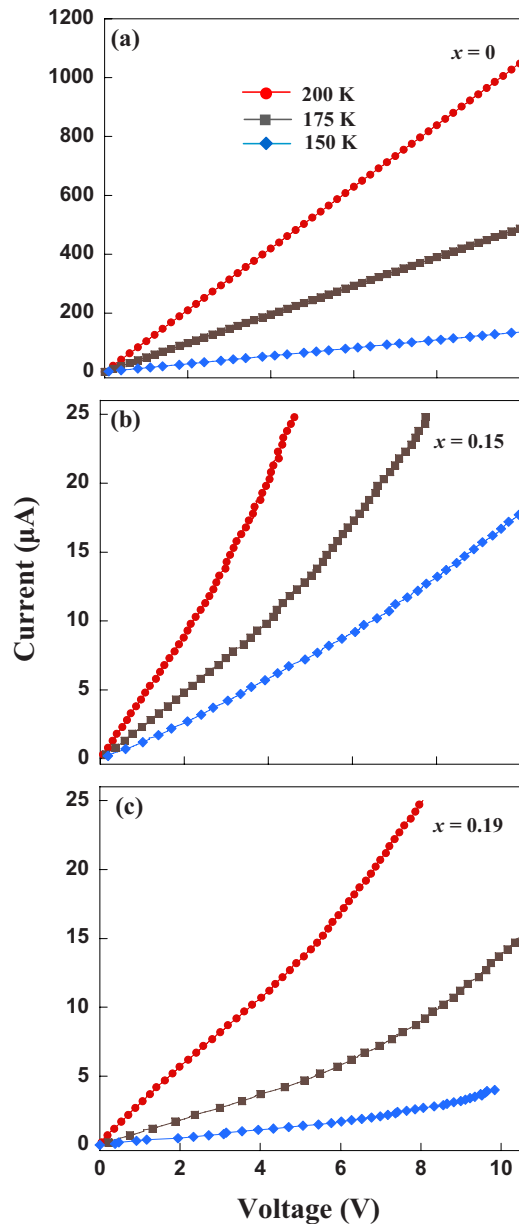


FIG. 5. (Color online)  $I$ - $V$  curves for  $(\text{Fe}_3\text{O}_4)_{1-x}(\text{Al}_2\text{O}_3)_x$  films as function of temperature for  $x=0$ ,  $x=0.15$ , and  $x=0.19$ , respectively.

function of  $x$ , with magnetic field applied parallel to the film of the plane. One of the striking features of the data is that the magnetization curves remain unsaturated even in magnetic fields above 8 kOe, although the magnetization is expected to saturate near the anisotropy field  $H_K$  of bulk  $\text{Fe}_3\text{O}_4$ ,  $\sim 310$  Oe.<sup>34</sup> This unsaturated behavior in high magnetic fields has been observed in epitaxial thin films of  $\text{Fe}_3\text{O}_4$  deposited on  $\text{MgO}$  and  $\text{Al}_2\text{O}_3$  substrates and has been interpreted as a consequence of antiphase boundaries (APBs).<sup>35–37</sup> Similar anomalous behavior was also observed in nanocrystalline  $\text{Fe}_3\text{O}_4$  films deposited on Si substrates by pulsed laser deposition,<sup>38</sup>  $\text{Fe}_3\text{O}_4$  films deposited by electron beam evaporation,<sup>26</sup> and  $\text{Fe}_3\text{O}_4$  films grown by dc magnetron sputtering.<sup>28,29,34</sup> By analogy to APBs, it has been suggested

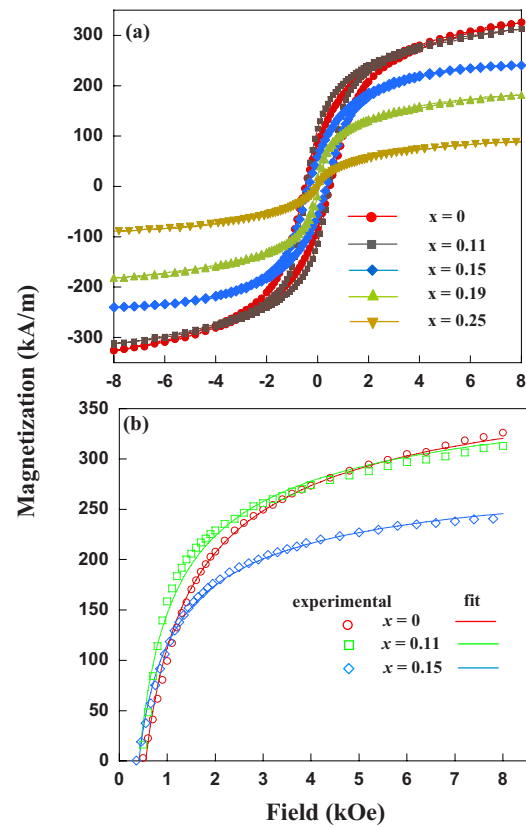


FIG. 6. (Color online) (a) In-plane experimental magnetization curves measured at room temperature, and (b) fitted magnetization curves for  $(\text{Fe}_3\text{O}_4)_{1-x}(\text{Al}_2\text{O}_3)_x$  films as a function of  $x$ .

that there exists AF coupling in the films through grain boundaries.<sup>26,28,29</sup> The existence of AF coupled regions makes it extremely difficult to align the spins near or at the boundaries in our films even in high magnetic fields.

The approach to saturation at high magnetic fields was fitted by<sup>37</sup>

$$M(H) = M_S \left( 1 - \frac{b}{\sqrt{H}} \right) \quad (5)$$

where  $M_S$  is the saturation field and  $b$  is a parameter which represents the difficulty of the approach to saturation. Figure 6(b) shows the magnetization curves for the  $(\text{Fe}_3\text{O}_4)_{1-x}(\text{Al}_2\text{O}_3)_x$  films fitted using Eq. (5). We obtained an extremely good agreement between the fits and the experimental magnetization curves. The  $M_S$  values estimated using Eq. (5) are 434, 409, and 317 emu/cm<sup>3</sup> for  $x=0$ ,  $x=0.11$ , and  $x=0.15$ , respectively. These  $M_S$  values are always lower than that of bulk  $\text{Fe}_3\text{O}_4$  (480 emu/cm<sup>3</sup>) at room temperature. Our results are thus consistent with the existence of a magnetically dead layer at the  $\text{Fe}_3\text{O}_4/\text{Al}_2\text{O}_3$  interface. As the  $\text{Al}_2\text{O}_3$  content in the granular films increases, there is an enhancement in the density of AF coupled grain boundaries as a consequence of grain size reduction.<sup>28</sup> This results in the reduction of saturation magnetization value with increasing  $x$ .

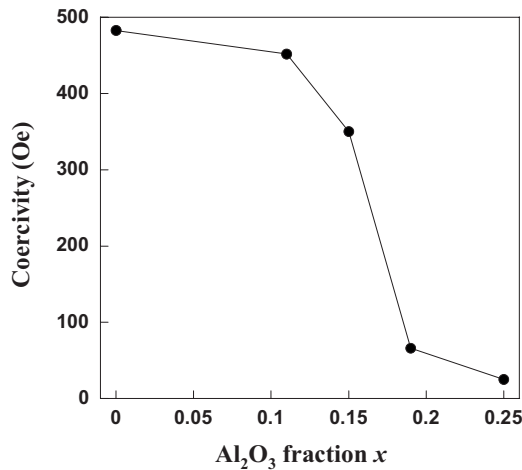


FIG. 7. Coercivity for  $(\text{Fe}_3\text{O}_4)_{1-x}(\text{Al}_2\text{O}_3)_x$  films as a function of  $x$ .

Another noticeable feature in the magnetization curves is the significant reduction in the coercivity  $H_c$  as the  $\text{Al}_2\text{O}_3$  content in the granular films is increased. Figure 7 shows the extracted values of  $H_c$  as a function of  $\text{Al}_2\text{O}_3$  volume fraction  $x$ . We observed that  $H_c$  decreases monotonically from 483 to 60 Oe as the  $\text{Al}_2\text{O}_3$  volume fraction is increased from  $x=0$  to  $x=0.19$ .  $H_c$  becomes almost negligible for  $x>0.19$ , with the magnetization curves exhibiting a typical Langevin curve.<sup>5</sup> This shows that for granular films having high  $\text{Al}_2\text{O}_3$  content, the  $\text{Fe}_3\text{O}_4$  grains are magnetically isolated and that the magnetization of these grains fluctuates by thermal agitation. This suggests that for large  $x$ , the magnetic properties of the  $(\text{Fe}_3\text{O}_4)_{1-x}(\text{Al}_2\text{O}_3)_x$  films may possibly be attributed to a superparamagnetic state. The coercivity in the  $\text{Fe}_3\text{O}_4$ - $\text{Al}_2\text{O}_3$  granular films is influenced by a variety of factors such as degree of ordering of ferromagnetic grains and the grain size. XRD results have confirmed that the intensity of the  $\text{Fe}_3\text{O}_4$  (311) peak becomes weaker with increasing  $x$ , indicating a reduction in the ordering. TEM and XRD observations have also revealed that the grain size decreases with increasing  $\text{Al}_2\text{O}_3$  content. Hence, it is reasonable that the coercivity of the films decreases with increasing  $x$ .

#### D. Magnetoresistance behavior

The magnetotransport properties of the  $(\text{Fe}_3\text{O}_4)_{1-x}(\text{Al}_2\text{O}_3)_x$  granular films have been systematically investigated as a function of  $x$ . Figure 8 shows the room-temperature MR curve for  $(\text{Fe}_3\text{O}_4)_{1-x}(\text{Al}_2\text{O}_3)_x$  films with  $x=0.11$ . The in-plane MR was measured with current parallel to the applied field (longitudinal MR) and perpendicular with respect to the applied field (transverse MR). It is evident that Figs. 8(a) and 8(b) are identical and no difference was observed between the two geometries. This shows the absence of any significant contribution from an anisotropic magnetoresistance effect. Such isotropic MR curves are typical of all our  $(\text{Fe}_3\text{O}_4)_{1-x}(\text{Al}_2\text{O}_3)_x$  granular films. We also observed that the maximum resistance occurs around the coercive field, which corresponds to the state of maximum disorder in

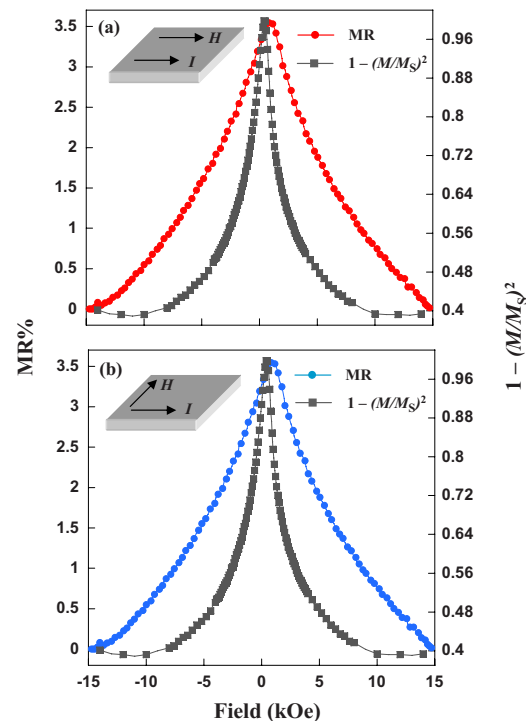


FIG. 8. (Color online) Magnetoresistance and  $\{1 - (M/M_S)^2\}$  measured at room temperature for  $(\text{Fe}_3\text{O}_4)_{1-x}(\text{Al}_2\text{O}_3)_x$  films for  $x=0.11$  with current (a) parallel to the applied magnetic field and (b) perpendicular to the applied magnetic field.

the orientation of the magnetic moments of neighboring grains. Hence, the magnetic field dependence of resistance, which is related to the alignment between grain moments, reaches a maximum. With increasing magnetic field, the grains tend to align ferromagnetically, thus resulting in low resistance. The observed MR is a granular TMR effect which can be attributed to the spin dependent tunneling of electrons across  $\text{Fe}_3\text{O}_4$  grains separated by insulating  $\text{Al}_2\text{O}_3$  barriers. It is worthwhile to compare this granular TMR effect in  $(\text{Fe}_3\text{O}_4)_{1-x}(\text{Al}_2\text{O}_3)_x$  films with the well known powder magnetoresistance (PMR) in pressed powder compacts of half metallic ferromagnetic oxides. The PMR effect is a variant of the TMR effect in which the oxide nanopowders represent ferromagnetic units, and contacts between the powders act as insulating tunnel junctions and ballistic point contacts, which permit spin polarized transport.<sup>39,40</sup>

For granular films with noninteracting grains, the MR has been compared with the global magnetization  $M$  to determine the existence of correlation between grains, and it has been suggested that MR should be proportional to  $\{1 - (M/M_S)^2\}$ .<sup>4</sup> We have calculated  $\{1 - (M/M_S)^2\}$  using the  $M_S$  values obtained from Eq. (5) and compared it with our MR curves. We note that this relation is not applicable to our  $(\text{Fe}_3\text{O}_4)_{1-x}(\text{Al}_2\text{O}_3)_x$  films, thus indicating that correlation between the grains should be considered. Such correlations could be mediated by direct exchange interactions which are expected to be ferromagnetic for small intergrain separations.<sup>41</sup> Among long range effects, dipole-dipole interactions are considered to be dominant but contribute both ferromagnetic and antiferromagnetic coupling.<sup>42</sup> The TMR

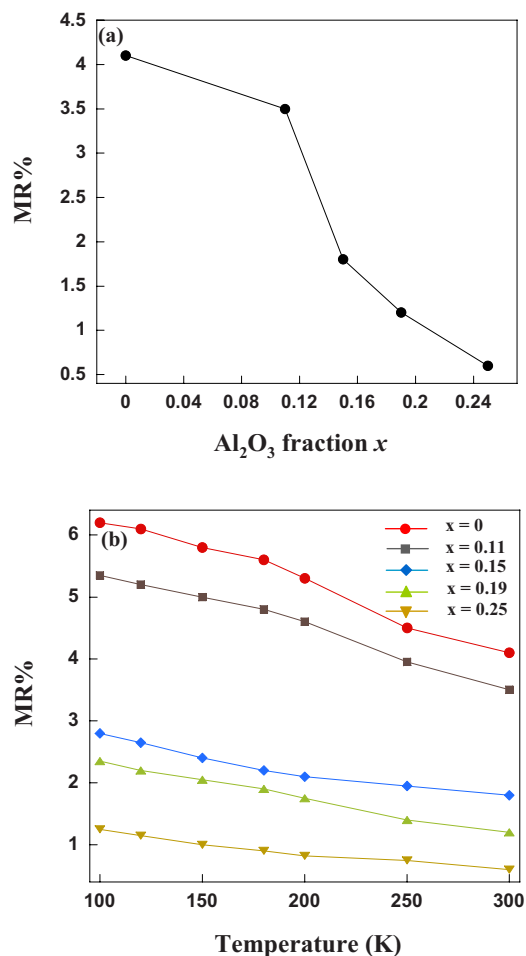


FIG. 9. (Color online) (a) Room-temperature TMR ratio measured as a function of  $x$ , and (b) temperature dependence of TMR ratio for  $(\text{Fe}_3\text{O}_4)_{1-x}(\text{Al}_2\text{O}_3)_x$  films.

results only from that fraction of  $\text{Fe}_3\text{O}_4$  grains which do not participate in the correlations mentioned above.

Figure 9(a) shows the room-temperature granular TMR ratio as a function of  $\text{Al}_2\text{O}_3$  content  $x$ . A large MR ratio which is expected from a highly spin polarized  $\text{Fe}_3\text{O}_4$  system is not observed for our  $(\text{Fe}_3\text{O}_4)_{1-x}(\text{Al}_2\text{O}_3)_x$  films. Liu *et al.*<sup>21</sup> have suggested that this reduction in MR ratio may be attributed to imperfect grain boundaries or grain-barrier interfaces, such as a magnetic dead layer, and a disordered spin structure. Moreover, the presence of traces of  $\text{Fe}^{3+}$  rich oxide in the  $\text{Fe}_3\text{O}_4$ - $\text{Al}_2\text{O}_3$  films greatly diminishes the spin polarization<sup>22</sup> and hence contributes further to the reduction in MR ratio. We also observed a monotonic decrease in the TMR ratio with increasing  $x$ , which may be attributed to an increase in the average width of the tunneling barrier. As a result, the conservation of the spin state of the conduction electrons in the tunneling barrier is broken down due to spin relaxation or by interactions with magnetic impurities in the tunneling barrier.<sup>4</sup> This weakens the effect of spin dependent

tunneling, and as a result, the TMR ratio also decreases. The temperature dependence of the TMR ratio for the  $(\text{Fe}_3\text{O}_4)_{1-x}(\text{Al}_2\text{O}_3)_x$  films is presented in Fig. 9(b). It is evident that the TMR ratio has a strong temperature dependence and decreases with increasing temperature for all the  $(\text{Fe}_3\text{O}_4)_{1-x}(\text{Al}_2\text{O}_3)_x$  films. A temperature dependent tunneling TMR may be attributed to various possible reasons. Firstly, a reduction in the spin polarization of the ferromagnetic materials with increasing temperature leads to a decrease of the tunneling TMR.<sup>43</sup> Although the magnitude of this effect is small for conventional ferromagnetic metal-insulator granular films such as  $\text{Fe-Al}_2\text{O}_3$  and  $\text{Fe-SiO}_2$ , it assumes significance for the  $\text{Fe}_3\text{O}_4$ - $\text{Al}_2\text{O}_3$  granular films due to the rapid decrease in the spin polarization of  $\text{Fe}_3\text{O}_4$  with increasing temperature due to finite-temperature spin disorder, thermally activated spin mixing, and magnon and phonon effects.<sup>44</sup> Moreover, the strong decrease of the TMR ratio with increasing temperature may also be due to spin-flip scattering,<sup>45</sup> which is caused by magnetic impurities in the tunnel barriers or by the excitation of bulk magnons. As temperature increases, the probability of spin-flip scattering increases and thus the TMR ratio also decreases.

#### IV. CONCLUSIONS

In summary, a systematic study of the structural, magnetic, and magnetotransport properties of an all-oxide  $\text{Fe}_3\text{O}_4$ - $\text{Al}_2\text{O}_3$  granular system prepared by cosputtering is presented in this paper. XRD and TEM analyses comprehensively show that with increasing  $\text{Al}_2\text{O}_3$  content, the  $\text{Fe}_3\text{O}_4$  grain size reduces drastically. We observed that the magnetic properties of the granular films closely follow the structural changes with coercivity and remanent magnetization of the films decreasing with increasing  $\text{Al}_2\text{O}_3$  content and the magnetization curves gradually changing from ferromagnetic to superparamagnetic. Temperature dependent resistance measurements and highly nonlinear  $I$ - $V$  characteristics confirm that the spin dependent tunneling of electrons featured by  $\log R \propto T^{-1/2}$  dominates the transport properties of the films. This tunneling transport causes an isotropic granular TMR effect in the granular films, the magnitude of which decreases with increasing  $\text{Al}_2\text{O}_3$  content due to increase in the tunnel barrier width. The TMR effect also exhibits strong temperature dependence and decreases with increasing temperature for all the granular films due to decrease in the spin polarization of  $\text{Fe}_3\text{O}_4$  and enhancement in the probability of spin-flip scattering processes.

#### ACKNOWLEDGMENTS

This work was supported by National University of Singapore (NUS) Grant No. R263-000-321-112/133. One of the authors (D.T.) would like to acknowledge NUS for his research scholarship. The authors would like to thank Jixuan Zhang from MSE department, NUS, for her cooperation in TEM imaging.

\*Corresponding author; eleaao@nus.edu.sg

- <sup>1</sup>M. N. Baibich, J. M. Broto, A. Fert, F. Nguyen Van Dau, F. Petroff, P. Etienne, G. Creuzet, A. Friederich, and J. Chazelas, *Phys. Rev. Lett.* **61**, 2472 (1988).
- <sup>2</sup>J. Q. Xiao, J. S. Jiang, and C. L. Chien, *Phys. Rev. Lett.* **68**, 3749 (1992).
- <sup>3</sup>A. Milner, A. Gerber, B. Groisman, M. Karpovsky, and A. Gladkikh, *Phys. Rev. Lett.* **76**, 475 (1996).
- <sup>4</sup>S. Mitani, H. Fujimori, and S. Ohnuma, *J. Magn. Magn. Mater.* **165**, 141 (1997).
- <sup>5</sup>S. Honda, T. Okada, M. Nawate, and M. Tokumoto, *Phys. Rev. B* **56**, 14566 (1997).
- <sup>6</sup>T. Zhu and Y. J. Wang, *Phys. Rev. B* **60**, 11918 (1999).
- <sup>7</sup>T. Furubayashi and I. Nakatani, *J. Appl. Phys.* **79**, 6258 (1996).
- <sup>8</sup>G. J. Strikers, H. J. M. Swagten, B. Rulkens, R. H. J. N. Bitter, W. J. M. de Jonge, P. J. H. Bloemen, and K. M. Schep, *J. Appl. Phys.* **84**, 2749 (1998).
- <sup>9</sup>P. Chen, D. Y. Xing, Y. W. Du, J. M. Zhu, and D. Feng, *Phys. Rev. Lett.* **87**, 107202 (2001).
- <sup>10</sup>R. A. de Groot and K. H. J. Buschow, *J. Magn. Magn. Mater.* **54-57**, 1377 (1986).
- <sup>11</sup>X. Li, A. Gupta, G. Xiao, W. Qian, and V. Dravid, *Appl. Phys. Lett.* **73**, 3282 (1998).
- <sup>12</sup>G. Hu and Y. Suzuki, *Phys. Rev. Lett.* **89**, 276601 (2002).
- <sup>13</sup>K. Ghosh, S. B. Ogale, S. P. Pai, M. Robson, E. Li, I. Jin, Z.-W. Dong, R. L. Greene, R. Ramesh, T. Venkatesan, and M. Johnson, *Appl. Phys. Lett.* **73**, 689 (1998).
- <sup>14</sup>S. S. P. Parkin, C. Kaiser, A. Panchula, P. M. Rice, B. Hughes, M. Samant, and S.-H. Yang, *Nat. Mater.* **3**, 862 (2004).
- <sup>15</sup>P. Seneor, A. Fert, J.-L. Maurice, F. Montaigne, F. Petroff, and A. Vaurès, *Appl. Phys. Lett.* **74**, 4017 (1999).
- <sup>16</sup>H. Matsuda, M. Takeuchi, H. Adachi, M. Hiramoto, N. Matsukawa, A. Odagawa, K. Setsune, and H. Sakakima, *Jpn. J. Appl. Phys., Part 2* **41**, L387 (2002).
- <sup>17</sup>K. Aoshima and S. X. Wang, *J. Appl. Phys.* **93**, 7954 (2003).
- <sup>18</sup>A. M. Bataille, R. Mattana, P. Seneor, A. Tagliaferri, S. Gota, K. Bouzehouane, C. Deranlot, M.-J. Guittet, J.-B. Moussy, C. de Nadaï, N. B. Brookes, F. Petroff, and M. Gautier-Soyer, *J. Magn. Magn. Mater.* **316**, e963 (2007).
- <sup>19</sup>A. M. Bataille, J.-B. Moussy, F. Paumier, S. Gota, M.-J. Guittet, M. Gautier-Soyer, P. Warin, P. Bayle-Guillemaud, P. Seneor, K. Bouzehouane, and F. Petroff, *Appl. Phys. Lett.* **86**, 012509 (2005).
- <sup>20</sup>A. M. Bataille, A. Tagliaferri, S. Gota, C. de Nadaï, J.-B. Moussy, M.-J. Guittet, K. Bouzehouane, F. Petroff, M. Gautier-Soyer, and N. B. Brookes, *Phys. Rev. B* **73**, 172201 (2006).
- <sup>21</sup>H. Liu, E. Y. Jiang, H. L. Bai, and R. K. Zheng, *J. Appl. Phys.* **95**, 5661 (2004).
- <sup>22</sup>W. Wang, M. Yu, M. Batzill, J. He, U. Diebold, and J. Tang, *Phys. Rev. B* **73**, 134412 (2006).
- <sup>23</sup>C. Park, Y. Shi, Y. Peng, K. Barmak, J.-G. Zhu, D. E. Laughlin, and R. M. White, *IEEE Trans. Magn.* **39**, 2806 (2003).
- <sup>24</sup>M. P. Klug and L. E. Alexander, *X-ray Diffraction Procedure for Polycrystalline and Amorphous Materials* (Wiley, New York, 1974), p. 634.
- <sup>25</sup>E. J. W. Verwey, *Nature (London)* **144**, 327 (1939).
- <sup>26</sup>D. Tripathy, A. O. Adeyeye, and C. B. Boothroyd, *J. Appl. Phys.* **99**, 08J105 (2006).
- <sup>27</sup>D. Tripathy, A. O. Adeyeye, C. B. Boothroyd, and S. N. Piramanayagam, *J. Appl. Phys.* **101**, 013904 (2007).
- <sup>28</sup>H. Liu, E. Y. Jiang, H. L. Bai, R. K. Zheng, H. L. Wei, and X. X. Zhang, *Appl. Phys. Lett.* **83**, 3531 (2003).
- <sup>29</sup>H. Liu, E. Y. Jiang, H. L. Bai, R. K. Zheng, and X. X. Zhang, *J. Phys. D* **36**, 2950 (2003).
- <sup>30</sup>C. Park, Y. Shi, Y. Peng, J.-G. Zhu, D. E. Laughlin, and R. M. White, *J. Appl. Phys.* **97**, 10C303 (2005).
- <sup>31</sup>P. Sheng, B. Abeles, and Y. Arie, *Phys. Rev. Lett.* **31**, 44 (1973).
- <sup>32</sup>S. Mitani, S. Takahashi, K. Takanashi, K. Yakushiji, S. Maekawa, and H. Fujimori, *Phys. Rev. Lett.* **81**, 2799 (1998).
- <sup>33</sup>L. F. Schelp, A. Fert, F. Fettar, P. Holody, S. F. Lee, J. L. Maurice, F. Petroff, and A. Vaures, *Phys. Rev. B* **56**, R5747 (1997).
- <sup>34</sup>D. T. Margulies, F. T. Parker, F. E. Spada, R. S. Goldman, J. Li, R. Sinclair, and A. E. Berkowitz, *Phys. Rev. B* **53**, 9175 (1996).
- <sup>35</sup>D. T. Margulies, F. T. Parker, M. L. Rudee, F. E. Spada, J. N. Chapman, P. R. Aitchison, and A. E. Berkowitz, *Phys. Rev. Lett.* **79**, 5162 (1997).
- <sup>36</sup>W. Eerenstein, T. T. M. Palstra, S. S. Saxena, and T. Hibma, *Phys. Rev. Lett.* **88**, 247204 (2002).
- <sup>37</sup>A. M. Bataille, L. Ponson, S. Gota, L. Barbier, D. Bonamy, M. Gautier-Soyer, C. Gatel, and E. Snoeck, *Phys. Rev. B* **74**, 155438 (2006).
- <sup>38</sup>J. Tang, K. Y. Wang, and W. Zhou, *J. Appl. Phys.* **89**, 7690 (2001).
- <sup>39</sup>J. M. D. Coey, *J. Appl. Phys.* **85**, 5576 (1999).
- <sup>40</sup>J. M. D. Coey, M. Venkatesan, and M. A. Bari, *Lect. Notes Phys.* **595**, 377 (2002).
- <sup>41</sup>Z. Celinski, B. Heinrich, and J. F. Cochran, *J. Appl. Phys.* **73**, 5966 (1993).
- <sup>42</sup>A. Gavrin, M. H. Kelley, J. Q. Xiao, and C. L. Chien, *Appl. Phys. Lett.* **66**, 1683 (1995).
- <sup>43</sup>J. S. Moodera, J. Nowak, and R. J. M. van de Veerdonk, *Phys. Rev. Lett.* **80**, 2941 (1998).
- <sup>44</sup>P. A. Dowben and R. Skomski, *J. Appl. Phys.* **95**, 7453 (2004).
- <sup>45</sup>F. Guinea, *Phys. Rev. B* **58**, 9212 (1998).